# Novel Near-Wellbore Fracture Diagnosis for Unconventional Wells Using High-Resolution Distributed Strain Sensing during Production

**G. Jin*,** Colorado School of Mines; **G. Ugueto,** Shell Exploration and Production Company; **M. Wojtaszek,** Shell International; **A. Guzik,** Neubrex Co., Ltd.; **D. Jurick,** Neubrex Energy Services; and **K. Kishida,** Neubrex Co., Ltd.

## Summary

The characteristics of hydraulic fractures in the near-wellbore region contain critical information related to the production performance of unconventional wells. We demonstrate a novel application of a fiber-optic-based distributed strain sensing (DSS) technology to measure and characterize near-wellbore fractures and perforation cluster efficiency during production. Distributed fiber-optic-based strain measurements are made based on the frequency shift of the Rayleigh scatter spectrum, which is linearly dependent on strain and temperature changes of the sensing fiber. Strain changes along the wellbore are continuously measured during the shut-in and reopening operations of a well. After removing temperature effects, extensional strain changes can be observed at locations around the perforation cluster during a shut-in period. We interpret that the observed strain changes are caused by near-wellbore fracture aperture changes caused by pressure increases within the near-wellbore fracture network. The depth locations of the measured strain changes correlate well with distributed acoustic sensing (DAS) acoustic intensity measurements that were measured during the stimulation of the well. The shape and magnitude of the strain changes differ significantly between two completion designs in the same well. Different dependencies between strain and borehole pressure can be observed at most of the perforation clusters between the shut-in and reopening periods. We assess that this new type of distributed fiber-optic measurement method can significantly improve understanding of near-wellbore hydraulic fracture characteristics and the relationships between stimulation and production from unconventional oil and gas wells.

## Introduction

US unconventional reservoirs have become major sources of global hydrocarbon production. In 2019, $2.83\times10^9$ barrels of crude oil and 25.3 trillion $ft^3$ of natural gas were produced from US shale reservoirs, equal to 9.6% of global oil production and 17.5% of global natural gas production, respectively. Production of low-permeability shale reservoirs has been enabled by horizontal drilling and hydraulic fracturing reservoir stimulation. The economics of unconventional reservoir development depends on reservoir properties and on well spacing and completion design. Many studies have been conducted to optimize well spacing and completion design through different means (Raterman et al. 2017, 2019; Zhu et al. 2017; Pankaj 2018).

The understanding of geometry and conductivity of hydraulic fractures can provide critical insights into optimization of well spacing and completion design. Many technologies have been developed to monitor and evaluate hydraulic fracturing results, including microseismic monitoring (Maxwell et al. 2010), time-lapse geochemistry (Liu et al. 2017, 2020a), electromagnetic imaging (Haustveit et al. 2017), and pressure analysis (Haustveit et al. 2017), as examples. More recently, hydraulic fracture monitoring based on distributed fiber-optic sensing has greatly advanced our understanding of fracture stimulation. DAS and distributed temperature sensing (DTS) are two commonly used distributed fiber-optic sensing technologies for hydraulic fracturing monitoring. DAS measures the distributed strain change or strain rate over a broad frequency range (1 mHz to several kHz), whereas DTS measures absolute temperature along the sensing fiber. Both technologies can provide meter to decameter range scale spatial measurements along the entire sensing fiber length. The sensing fiber can be installed in the stimulated well (in-well) or offset monitor wells (cross well). Depending on the application, fiber cable can be permanently installed behind the casing or temporarily installed through wireline or coiled-tubing intervention (Richter et al. 2019).

DAS has been used to monitor the acoustic intensity of flow noise at perforation clusters during hydraulic fracturing injection operations. The acoustic noise level at each perforation cluster location can be used to estimate or allocate injection volume among the clusters of the same treatment stage (Molenaar et al. 2012). However, there are various ideas about the cause of the acoustic noise and its relation to the cluster injection rate (Stokely 2016; Friehauf and Gibson 2019; Ugueto et al. 2019a). DAS can also be used to monitor microseismic events (Karrenbach et al. 2017; Cole et al. 2018; Vera Rodriguez and Wuestefeld 2020), to perform time-lapse vertical seismic profiles (Byerley et al. 2018; Binder et al. 2019; Titov et al. 2020), and to measure cross-well strain variation (Jin and Roy 2017). Such measurements have been used in an attempt to measure and estimate the far-field hydraulic fracture geometry. During the life cycle of a well, DAS can provide production allocation estimates for certain types of unconventional wells (Ugueto et al. 2018; Jin et al. 2019). DTS can be used to evaluate stage isolation and plug integrity during stimulation. It can also be used to estimate production allocation during producing periods (Jin et al. 2019). By monitoring formation warmback after the stimulation, DTS data can also help to constrain the geometry of near-wellbore fractures (Raterman et al. 2019; Ugueto et al. 2019a).

There is another type of distributed fiber-optic sensing technology that has not yet been widely adopted by the oil industry, which is DSS. DSS can monitor absolute strain or long-term strain change along a sensing fiber. Traditionally, distributed strain measurement is made through estimating the value of frequency, often called center frequency, of Brillouin scattering. The center frequency is sensitive to both absolute temperature and strain of the fiber (Horiguchi et al. 1989). By combining Brillouin measurements with DTS measurements or other independent temperature measurements, absolute strain along the fiber can be estimated. Brillouin-based DSS

*Corresponding author; email: gjin@mines.edu



Original SPE manuscript received for review 23 November 2020. Revised manuscript received for review 31 January 2021. Paper (SPE 205394) peer approved 22 February 2021.

measurements have been used to monitor strain changes of physical infrastructure elements and pipelines (Guzik et al. 2013), as well as to monitor formation overburden and wellbore casing deformation (Mali et al. 2019). The challenge of this Brillouin-based method is that the precision is too low because the Brillouin gain spectrum width is too wide. The sensitivity of Brillouin optical time domain reflectometry type of DSS measurements can only reach a few tens of microstrain units, which is not adequate for some borehole-measurement-based objectives and applications. More recently, another type of DSS measurements based on weak fiber Bragg grating (FBG) was developed and applied to monitor long-term reservoir and overburden deformation caused by pressure depletion. This technology can provide microstrain-level sensitivity, but the commercially available solutions are often limited by the length of the sensing portion of the fiber, because only a limited number of FBGs can be deployed in a single fiber (Kole et al. 2017).

After the initial finding of DAS cross-well responses by Webster et al. (2013), Jin and Roy (2017) discovered that the low-frequency DAS signal (LF-DAS) can be used as a hybrid DSS to monitor strain perturbation induced by hydraulic fracture propagation at offset monitor wells. Many field studies have been conducted on this DAS application (Karrenbach et al. 2019; Ugueto et al. 2019b; Ichikawa et al. 2020; Liu et al. 2020b). LF-DAS can measure fractional microstrain changes; however, the spatial resolution is limited by the gauge length configuration of the system, which is usually larger than 1 m, partially to ensure good signal-to-noise ratio and signal quality. Most of the LF-DAS studies in unconventional reservoirs focus on strain changes at offset monitor wells during stimulation. Little attention has been paid to in-well strain changes during production periods, because of the limitation of current DSS solutions.

During production, pressure depletion within the hydraulic fractures and reservoir matrix can cause long-term, permanent stress changes in hydraulically fractured reservoirs. The stress changes sometimes affect the fracture propagation of subsequent refracturing and infill well stimulation operations (Wang 2016; Rezaei et al. 2017). On the other hand, short-term reservoir stress changes are expected to be induced by sudden borehole pressure perturbation; for example, the pressure buildup caused by temporary well shut-ins. The temporary shut-in-induced stress changes are, in general, concentrated near the wellbore, which are closely related to the fractures in the near-wellbore region. If a sensing fiber-optic cable is deployed along the producing borehole, the strain induced by the stress changes can be detected and measured. The measured strain can then be used to constrain near-wellbore fracture characteristics, which are critical for understanding the production performance of unconventional reservoirs and wells, because all produced fluid flows through the near-wellbore regions before it enters the borehole.

In this work, we present a field-based example of a new type of DSS measurement from an unconventional producing well during a shut-in operation. This work is part of the Hydraulic Fracture Test Site 2 project, which is a joint industry partnership research experiment performed in the Permian-Delaware Basin, West Texas, USA. In the following sections, we first introduce the measuring principle of this novel DSS method and then present the field results measured and acquired during a shut-in and reopening operation of a hydraulically fractured producing well. Then, we present interpretations of the measurements and potential applications. Finally, we conclude with our findings and assessments.

## DSS Method

The DSS based on the Rayleigh frequency shift (RFS) method (Kishida et al. 2014) uses Rayleigh backscatter in a regular nonengineered single-mode fiber to measure strain change along a fiber. It is different from the three aforementioned DSS methods in terms of measuring principles. It has a higher measuring sensitivity ($<1\ \mu\varepsilon$) than the Brillouin optical time domain reflectometry method, a higher spatial resolution (20 cm for a 8-km fiber) compared to DAS systems, and does not have restrictions on sensing fiber length like commercially available weak FBG-based DSS systems. Similar to DAS and weak FBG-based DSS, it measures relative strain changes instead of absolute strain along the fiber.

The principle of the DSS-RFS method is described as follows. When an optical fiber is manufactured, random inhomogeneities of the glass density are imprinted into the fiber core. The random density heterogeneities manifest themselves as a fluctuation of refractive index along the fiber. For a certain laser frequency, the constructive and destructive interferences between the Rayleigh backscatterers of the density fluctuations cause irregular amplitude fluctuation in the coherent optical time-domain reflectometer along the fiber length. For each unique and discrete fiber section, a unique Rayleigh scattering spectrum is obtained by scanning the fiber with coherent optical time-domain reflectometer with a range of laser frequencies using a tunable-wavelength laser system. The Rayleigh scattering spectrum shifts in frequency if the temperature and/or strain of the fiber section changes, which causes the spacing and optical delay to vary between the scatterers. The measuring principle is conceptually demonstrated in **Fig. 1.**

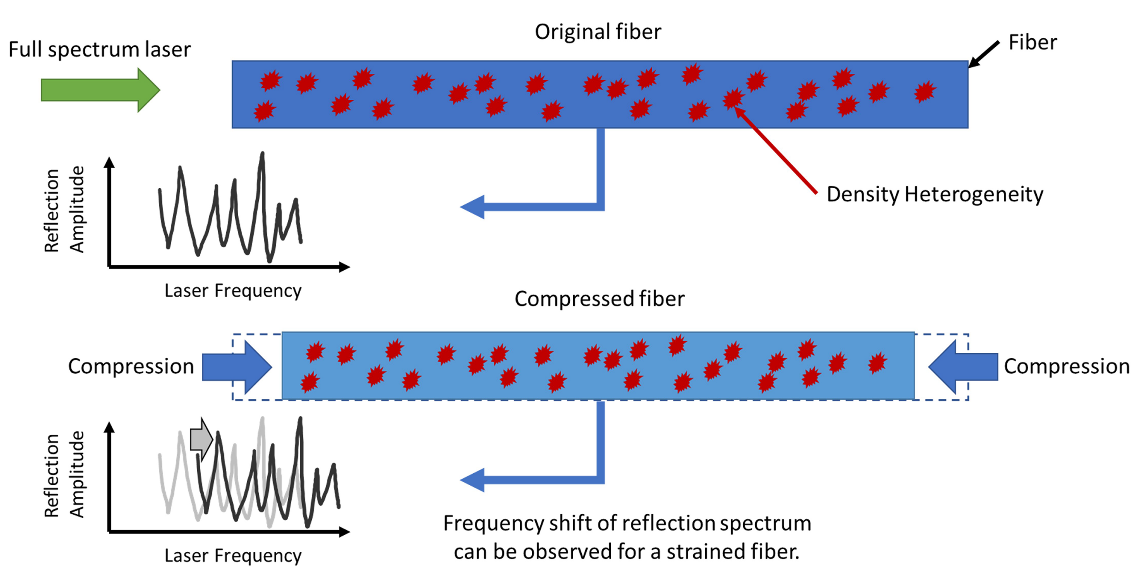


**Fig. 1—Conceptual illustration of an RFS measurement. The frequency shift of the Rayleigh reflection spectrum is linearly dependent on fiber temperature and strain changes.**

The relationship between Rayleigh spectrum frequency shift and temperature and strain variations is presented as:

$$\Delta \nu_R = C_1 \Delta \varepsilon + C_2 \Delta T, \quad (1)$$

where $\Delta \nu_R$ is the frequency shift of the Rayleigh scattering spectrum at a certain section of the sensing fiber, which is referred to as RFS in this article. $\Delta \varepsilon$ and $\Delta T$ are the strain and temperature variations of the fiber section under study, respectively. $C_1$ and $C_2$ are coefficients determined by fiber structure and materials. $C_2$ can be significantly different for fibers that are embedded in protective cables, because it is dependent on the thermal expansion coefficient of the entire structure that are mechanically coupled with the sensing fiber.

Although RFS can be caused by either temperature or strain variations, the temperature variations can be independently measured using DTS on a multimode fiber in the same cable as the RFS sensing fiber. It is noted that there is a major sensitivity difference between an RFS measurement and a DTS measurement. If the temperature variation can be accurately measured or is small enough to be ignored, then the strain changes can be measured in a fully distributed manner using the RFS. Because the pattern of the Rayleigh scattering spectrum is unique for each section of sensing fiber and does not change over time, the pattern can be used to recognize fiber location and strain changes in the sequential data acquisitions. This enables long-term time-lapse strain change monitoring using the DSS-RFS method without the continuous and ongoing measurements.

It is worth noting that the sensing method of DSS-RFS measurement is fundamentally different from DAS-based strain measurement. The DSS-RFS method measures amplitudes of Rayleigh scatter at different laser frequencies, although DAS measures phase differences of single-frequency Rayleigh scatter. The two types of measurements differ in spatial and temporal resolutions because of their measuring principles. DSS-RFS measurements have a higher spatial resolution but a lower temporal resolution compared to DAS measurements. The DSS-RFS measurements have been used to monitor shallow-water injection (Xue and Hashimoto 2017). To the best of our knowledge, this is the first reported field application of DSS-RFS technology on a producer that is hydraulically fractured.

## Data Acquisition and Results

Data are acquired at one of the instrumented wells of Hydraulic Fracture Test Site 2. The RFS is measured on a single-mode fiber using a Neubrex® SR7000 (Neubrex Co. Ltd., Hyogo, Japan) Rayleigh interrogator unit, which has a sensitivity of 0.075 GHz, equivalent to 0.5 $\mu\varepsilon$ or 0.06°C. The spatial resolution of the measurement is 20 cm, with a time sampling interval of 150 seconds. This time sampling interval setting is much longer than the instrument specification (8 seconds for 10-km fiber) because of the strong reflection at the fiber end. The fiber cable is clamped to the outside of casing and cemented in place. In this study, we assume the sensing cable is mechanically fully coupled with the surrounding rocks. The fiber is placed in a metal tube filled with thixotropic gel, which can transfer short-term shear strain changes. A DTS interrogator is connected to a multimode fiber in the same cable to measure distributed temperature along the cable on a 5-minute time measurement interval, with a spatial resolution of 1 m.

The data acquisition in this study began when the instrumented well was under stable production conditions approximately 8 months after initial production. After establishing a baseline measurement during open flow production, the well was shut in for 4 days and then opened again after a series of 2-hour shut-in and 1-hour producing cycles. The data acquisition stopped 6 hours after the final opening. The acquired RFS and DTS data are shown in **Fig. 2** along with downhole pressure gauge measurements. The DTS data are converted from absolute temperature to temperature change by removing the temperature baseline measured during the stable production period at the beginning of the field experiment. It is observed that the DTS and RFS data follow the same trend in the vertical section (less than 3,500 m of measured depth). However, a significant difference is observed in the horizontal section of the well between the RFS and DTS measurements. Because DTS is insensitive to pressure or strain changes, the observed difference is interpreted to be due to mechanical strain changes.

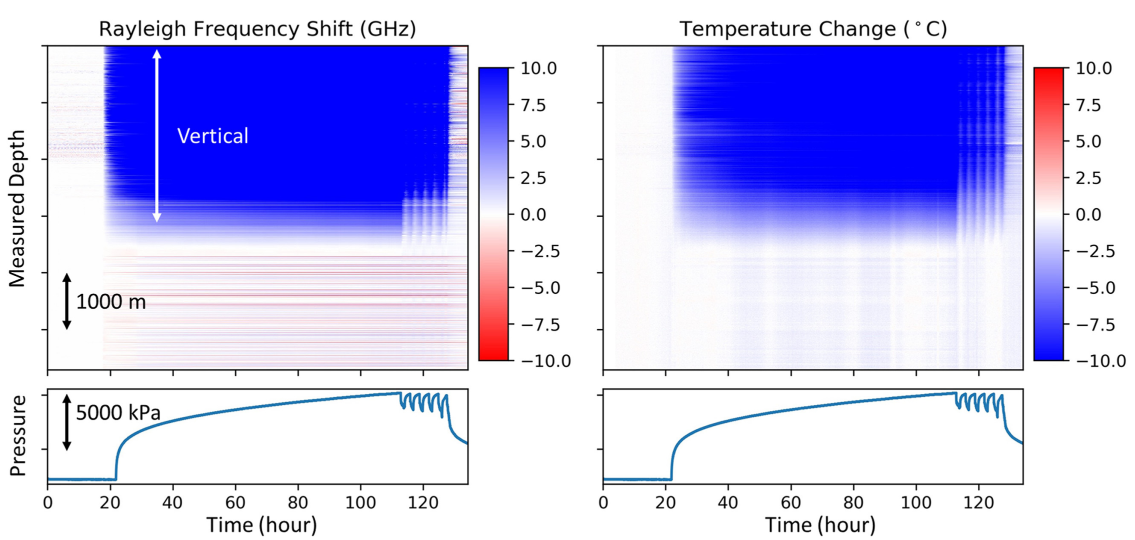


**Fig. 2—RFS (left panels) and DTS (right panels) measurements compared with borehole pressure gauge data (bottom panels). The DTS measurement is shown as temperature changes by removing the baseline temperature measured during stable production. The color bar of the RFS measurement is reversed to match the DTS plot.**

To further investigate the difference between the two measurement types, the averaged profiles of RFS and DTS temperature changes along the wellbore depth are calculated. The profiles are obtained by averaging 24 hours of RFS and DTS measurements during the last day of the shut-in period. The averaging process is performed to reduce the noise of DTS data to match the sensitivity of RFS measurement. The averaged borehole temperature change between shut-in and stable production from DTS measurement is then converted to corresponding RFS, using a coefficient of −1.5 GHz/°C. The comparison between the measured RFS and the DTS predicted temperature-induced RFS is shown in the upper panel of **Fig. 3.** The RFS measurement and temperature-induced RFS correlate well in the vertical section. In the horizontal section within the perforation zone, RFS shows a much larger spatial variation than the DTS measurement, indicating the influence of mechanical strain change effects, which can be calculated by removing the temperature effect using the DTS measurement. The strain change is calculated using:

$$\Delta\varepsilon = \frac{\Delta\nu_R - C_2\Delta T}{C_1}, \qquad (2)$$

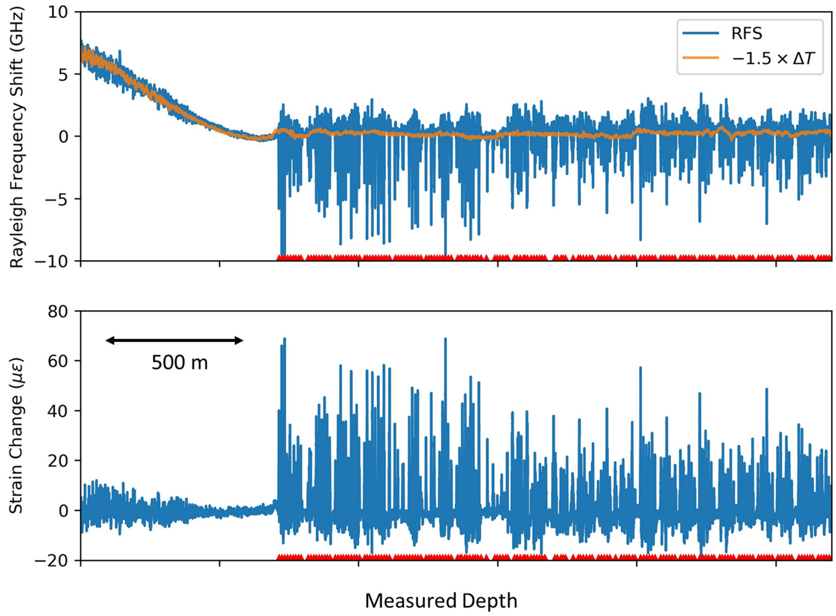


**Fig. 3—The top panel shows the averaged RFS compared with predicted temperature-induced RFS from DTS temperature change measurement. The bottom panel shows the mechanic strain change after remove the temperature influence from the RFS measurement. The red triangles at the bottom of each plot indicate the locations of perforation clusters.**

The calculated strain change is shown in the lower panel of Fig. 3. Strain changes are close to zero outside perforated zones, which indicates the effectiveness of the temperature effect removal process. Clear positive (extensional) strain changes are observed at the perforation cluster locations, which is better illustrated in a zoomed-in plot of one stage shown in **Fig. 4,** where individual positive strain peaks can be identified at most perforation cluster locations.

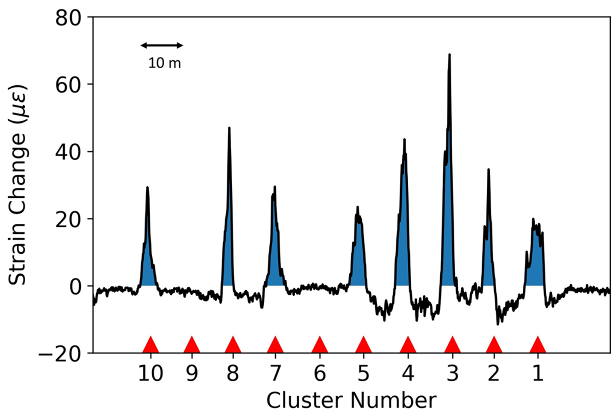


**Fig. 4—Mechanical strain change between shut-in and stable production at stage A. The red triangles show the perforation cluster locations. A positive strain indicates extension.**

The positive (extensional) strain change after a temporary shut-in (for example, 3 to 4 days) can be interpreted as the aperture of near-wellbore fracture increases caused by pressure recharging. During stable production, the fluid pressure within the hydraulic fractures is lower than the rock matrix pore pressure because of the continuous production. The pressure difference generates mechanical stress on fracture surfaces and reduces fracture aperture through elastic deformation. After the shut-in, the pressures in the fracture and the matrix pore space begin to equilibrate, decreasing the pressure drawdown between the reservoir matrix and fracture fluid, leading to an increase of fracture aperture. This elastic mechanical response generates strain perturbations near the producing hydraulic fractures, which are detected and captured by the DSS-RFS measurements. An illustration of the proposed conceptual model is shown in **Fig. 5.** Although this fracture aperture change during shut-in may happen along the entire connected fracture length, the measured strain changes are primarily affected by the aperture change of near-wellbore fractures because the sensing fiber is deployed along the production well. Distributed and simultaneous measurements are made along the entire wellbore length and continuously over the monitoring period.

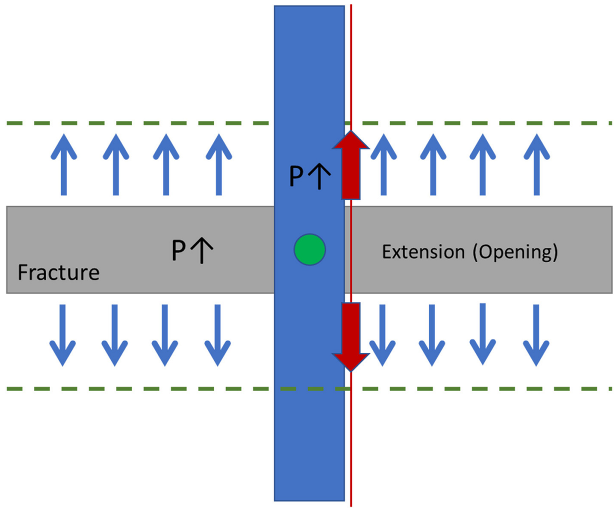


**Fig. 5—Conceptual model of positive strain change observed at perforation clusters.**

The RFS measurements were taken every 150 seconds over the entire acquisition period. Time-dependent relationships between borehole pressure and strain changes at perforation cluster locations are further investigated for understanding near-wellbore fracture properties. **Fig. 6** shows a comparison between the strain change at a perforation location and borehole pressure measurements. It is seen that although the strain measurements follow the borehole pressure variations closely in general (upper panel), a significant difference in terms of strain-pressure change ratio is observed during the shut-in and opening period. The interpretation of the difference will be discussed in the following section.

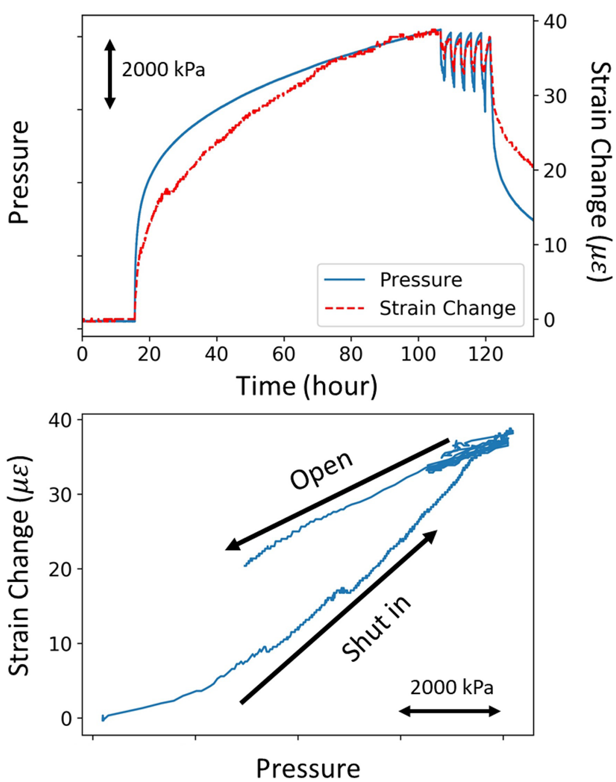


**Fig. 6—Strain change at a perforation cluster location compared with borehole pressure measurement.**

The time-dependent strain changes shown in Fig. 6 are calculated directly from RFS measurement without DTS correction. This approach is considered reasonable by the authors in this example because the effect of temperature variation in the horizontal section is much smaller than the mechanical strain change (less than 10% as shown in Fig. 3), and the DTS data are too noisy to be directly compared with RFS without a long-term averaging.

## Discussion

The spatial resolution of the DSS-RFS measurement is 0.2 m, which is larger than commonly believed hydraulic fracture aperture but much smaller than the extensional strain signals observed at perforation cluster locations during the shut-in period. The extensional strain signals have an average width of 3 to 5 m (Fig. 4), significantly wider than the spatial distribution of perforation holes at each cluster (0.3 to 0.6 m). We interpret the regions with extensional strain signals as the near-wellbore regions that are highly conductive and connected to the wellbore through the perforations. These regions likely consist of conductive hydraulic fracture swarms that are created during stimulation. In this study, we refer to these regions with extensional strain signal as "near-wellbore fracture zones." We acknowledge that there may be hydraulic fractures between these fracture zones, but they are unlikely to be directly connected to the wellbore and are not of interest in this study.

In this section, we first compare the DSS-RFS measurements with DAS acoustic noise measurements during the injection. Next, we discuss how the near-wellbore fracture zones are affected by the number of clusters per stage and the cluster spacing designs. We then discuss the relation of the strain response with borehole pressure measurement. We conclude this section by discussing the limitations and potential future applications of this new technology.

**Cluster Efficiency and DAS Acoustic Intensity Comparison.** The acoustic intensity of the DAS signal during hydraulic fracture stimulation can serve as a good estimate of perforation cluster efficiency and injectivity, because higher DAS acoustic intensity levels at cluster locations during injection may indicate more slurry intake (Molenaar et al. 2012). **Fig. 7** shows the comparison between the DAS acoustic intensity measurements during stimulation and DSS-RFS measurements after 8 months of production for two treatment stages. In stage A, very limited injectivity can be observed at Clusters 6 and 9 (marked by red dots in Fig. 7) during stimulation, and no positive strain changes are observed in the DSS-RFS data. The same type of correlation is found at stage B, which has one skipped perforation cluster between Clusters 4 and 5.

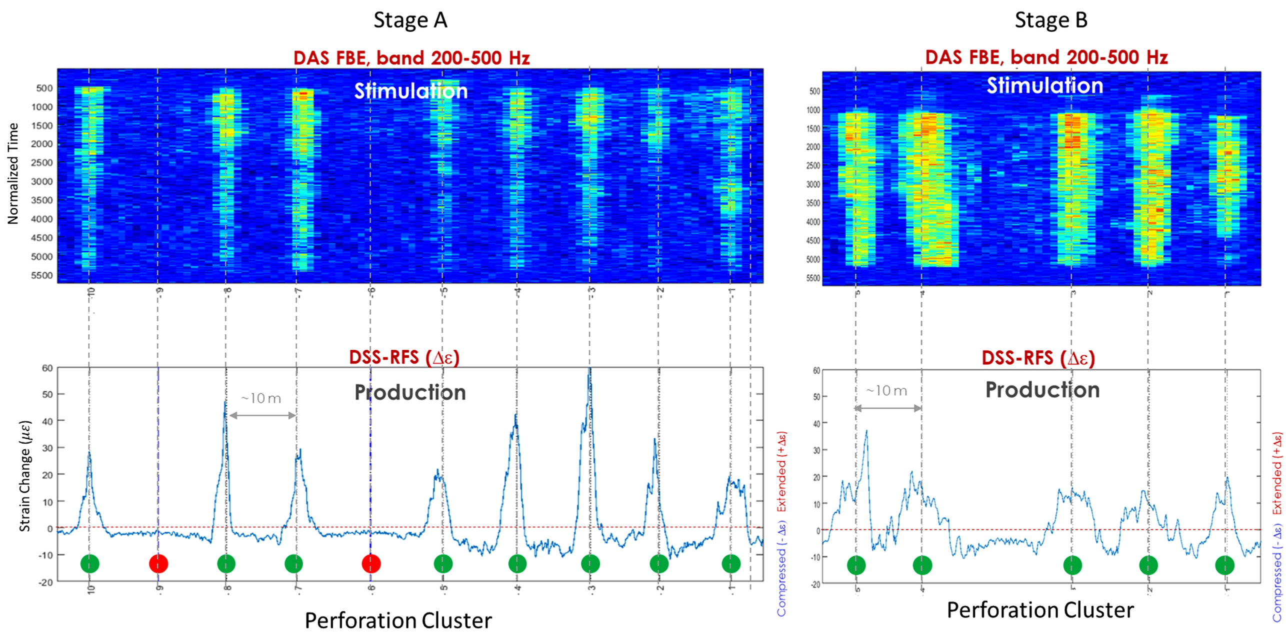


**Fig. 7—Comparison between DSS-RFS measurement with DAS acoustic intensity measurement during stimulation. The top panels are waterfall plots for DAS acoustic intensity at 200- to 500-Hz frequency band. The bottom panels show strain change during the shut-in, a similar plot as shown in Fig. 3. The left and right panels are from two different stages of the instrumented well. The warmer color bar indicates higher noise level during injection. The dashed lines highlight the perforation locations. The red horizontal dashed line marks the level of zero strain. The red dot and green dot illustrate inefficient and efficient perforation clusters, respectively. FBE = frequency bands extracted.**

The hydraulic fractures that generate extensional strain responses during shut-in operations are the ones that are hydraulically connected to the wellbore. Therefore, the strain change can serve as a qualitative evaluation for perforation cluster efficiency. The clusters that do not develop a positive strain change during shut-in are less likely to be the clusters that contribute to wellbore production because of the lack of hydraulic fracture connectivity to the reservoir.

A strong spatial correlation between the two data sets (DAS during stimulation and DSS-RFS during production shut-in period 8 months after the start of the production) is observed at the individual perforation cluster level, as well as along the entire stimulated wellbore. In Fig. 7, the borehole regions with high DAS acoustic intensity signal in Stage B, at each cluster, are significantly wider than the ones in Stage A. A similar trend can be observed in the strain change measurements, with positive strain peaks in Stage B being wider and of smaller magnitudes. Because the spatial distributions of perforation holes at each cluster are similar between these two stages, this observation supports the interpretation of Ugueto et al. (2019a), who hypothesized that part of the DAS acoustic intensity signals during stimulation is generated by near-wellbore region instead of at perforation entry alone. The spatial consistency between the DAS acoustic intensity during stimulation and strain change during production indicates that DAS acoustic intensity is likely to be more associated with near-wellbore fractures behind casing than the pressure drop across the perforation orifice or entry points at the perforation clusters. This also explains the spatial migration of DAS acoustic intensity signal near the perforation clusters during stimulation, which is commonly observed and are clearly seen at Cluster 5 of Stage B in Fig. 7. On the other hand, the consistency of the DSS-RFS measurements with the DAS intensity during injection also supports our interpretation that the extensional strain signals during shut-in are associated with highly conductive near-wellbore fracture zones that are created during stimulation.

**Near-Wellbore Fracture Network and Cluster Number per Stage.** The shape and magnitude of the strain change curve can be attributed to the geometry and connectivity of near-wellbore fracture zones. As shown in Figs. 3 and 7, the average width of positive strain regions associated with each perforation is approximately 3 to 5 m, with a clear zero to negative strain region between the perforation clusters. Moreover, the total aperture change of each near-wellbore fracture zone can be estimated by integrating the measured strain value within the positive strain change region at each perforation cluster (the blue area in Fig. 4). We observe a strong dependence of near-wellbore fracture aperture change on completion designs implemented at the monitored well. **Fig. 8** shows the distribution of maximum strain change and the increase of fracture aperture at each perforation cluster location grouped by two different stimulation completion designs, that Design 1 has fewer clusters per stage than Design 2. The larger strain response and fracture aperture change of Design 2 may be associated with lower average injection rate at each perforation cluster because of the higher cluster number per stage during stimulation. A lower slurry rate could also change proppant transportation capability, especially in the near-wellbore region, and therefore may lead to different geometry and other properties of the high-conductive near-wellbore fracture zones.

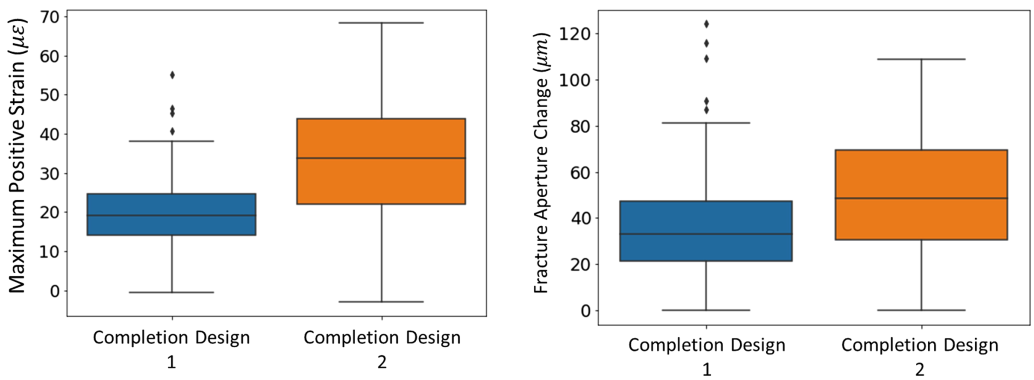


**Fig. 8—Distribution of measured maximum positive strain change (left panel) and fracture aperture change (right panel) at perforation clusters, grouped by different completion designs of the instrumented well. The top and bottom whiskers show the maximum and minimum values that are not outliers. The outliers are marked by black dots. The top and bottom edges of the solid box show the 25th and 75th percentile of the values. The solid horizontal line near the center of each solid box marks the median value.**

**Cluster Spacing.** We assess that the spatial distribution of conductive near-wellbore fracture zones is heavily influenced by cluster locations, because there is little to no positive strain change that is observed in the near-wellbore region between the clusters (Fig. 4). This result is not consistent with reservoir interval core analysis reported by Raterman et al. (2017), in which observed hydraulic fractures at some distance from the stimulated wellbore, in post-fracture stimulated cores, are much denser than the cluster spacing, and the existence of hydraulic fractures between the clusters is abundant. Raterman et al. (2017) also reported that hydraulic fracture hits with a spacing close to cluster spacing are seen in the far-field measurements using LF-DAS signals. Although the analyses of Raterman et al. (2017) along with the results presented here were conducted in different reservoirs, the comparison between the two sheds light on the properties of hydraulic fractures. Both cross-well LF-DAS measurements and in-well DSS-RFS strain change measurements detect and quantify strain variations induced by hydraulic fracture aperture changes caused by pressure perturbation (by injection or shut-in operations). Therefore, both measurements are only sensitive to the hydraulic fractures that are conductive and connected to the borehole. Combined with the core observation and assuming a similar hydraulic fracture geometry in both studies, it is reasonable to hypothesize that a dense hydraulic fracture network may be generated during hydraulic fracture stimulation; however, conductive fracture zones are relatively sparse, with a spacing that is heavily influenced by cluster spacing. The in-well DSS-RFS measurements, combined with cross-well fracture hit measurements during stimulation, can provide important insight on cluster spacing design decisions. With low reservoir permeability, an optimized cluster spacing is the one that creates the most effective conductive hydraulic fractures in both the near-wellbore and the far-field regions of the reservoir and with good connectivity to the wellbore. However, hydraulic fracture geometry can be affected by in-situ stresses and existence of natural fractures. For the reservoirs with more complex hydraulic fracture geometry, the same conclusion may not be valid.

**Time-Dependent Pressure-Strain Relation.** Strain changes at each perforation location are continuously monitored during the shut-in operation at a sampling interval of 150 seconds. Assuming that the observed strain changes are due to elastic deformation of near-wellbore fractures responding to pressure change, the measurements can serve as proxy to the pressure changes in the near-wellbore fracture zones. During the shut-in period of a multicluster horizontal well, the interaction between the borehole and the near-wellbore fractures can be complicated because of various conductivities between borehole and near-wellbore fractures combined with different recharging rates by the reservoir matrix. Cross-flow within the wellbore can also be generated from the better connected and faster-recharging fractures to those that are poorly connected and slowly recharged. After the well is reopened, fractures with lower connectivity or higher recharging rates to the borehole may show larger discrepancy on borehole pressure-strain relationship curves between the shut-in period and reopening period, as illustrated in the lower panels of Fig. 6 and **Fig. 9.** Strain responses can be history matched by reservoir simulation modeling to quantitatively constrain the near-wellbore fracture properties and reservoir. Building such simulation models is beyond the scope of this work but will be conducted in future studies.

**Limitations and Potential Applications.** Like all technologies, the DSS-RFS method has its own advantages and disadvantages. Compared with the Brillouin-based DSS system, the DSS-RFS system has a much higher sensitivity but can only measure relative strain changes instead of absolute strain distribution along the fiber. Compared with the weak FBG-based DSS system, the DSS-RFS system can measure much longer fiber sections but has relatively lower spatial resolution for long-range measurements. Compared with LF-DAS measurements, the DSS-RFS system has higher spatial resolution but lower temporal resolution. It is also more sensitive to high-frequency vibrations of the sensing fiber and cannot provide reliable measurements in extremely noisy environments. All DSS measurements are sensitive to temperature changes and rely on other independent temperature measurements, usually DTS, to remove the thermal effect. Borehole DSS measurements also heavily depend on the mechanical coupling of the sensing fiber and formation rocks, which depends on both cable installation and cable designs. Most of the current borehole fiber-optic cable designs use metal tubes filled with thixotropic gel to protect sensing fiber. The liquid thixotropic gel can transfer short-term strain changes but relaxes any residual strain on the fiber over a long period of time. Dedicated cables for strain sensing are commercially available but have not been commonly installed in unconventional wells.

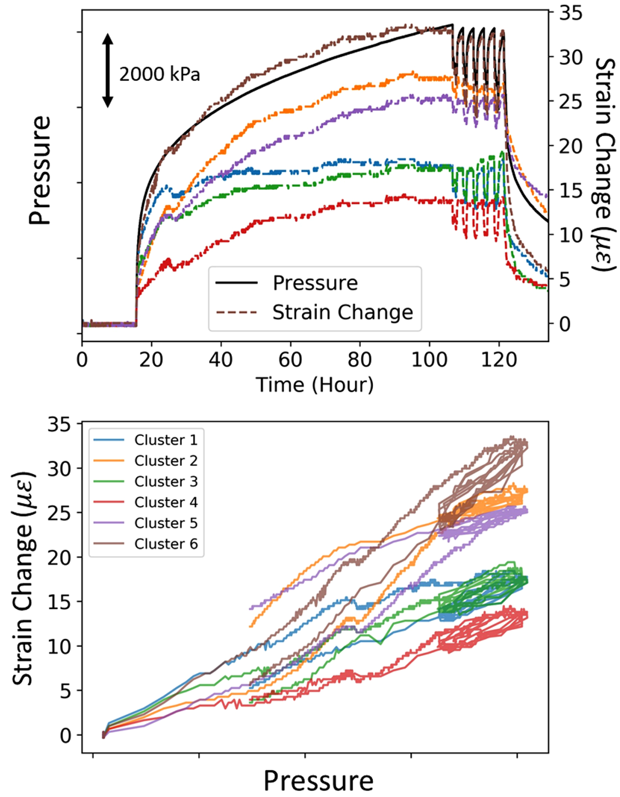


**Fig. 9—Pressure and strain change relation for multiple perforation clusters of the same stage.**

If the pressure depletion is rapid or if a strain-sensing cable is installed, DSS-RFS can be used to monitor the aperture decreasing in near-wellbore fractures during production. This can provide similar strain change measurements without shut-in operations, except the expected strain change is negative (compressional) at perforation cluster locations. DSS-RFS can also be used for cross-well strain measurement during stimulation. With the higher spatial resolution, the measurements are expected to provide more details of the fracture-hit signals than LF-DAS measurements (Jin and Roy 2017).

## Conclusions

We present a new technology that uses fiber-optic-based DSS-RFS methods to evaluate near-wellbore fracture characteristics of an unconventional reservoir and well during production. Strain variations along the borehole are shown to be related to borehole pressure changes at each perforation cluster with high spatial resolution and temporal sampling rates during shut-in and reopening well operations. The strain variations are interpreted to be the result of near-wellbore fracture aperture changes over time and space. The shape and magnitude of the strain change peaks are related to the geometry of conductive near-wellbore fracture zones. Importantly, significant differences can be observed for the two different types of stimulation completion designs of the monitored well. The time-dependent relation between borehole pressure and strain change provides important insights into near-wellbore fracture conductivity and reservoir recharge rate. The innovation described here in using distributed fiber-optic strain sensing measurements will improve understanding of the near-wellbore hydraulic fracture characteristics and the interaction between stimulation design and production yield in unconventional reservoirs.

## Acknowledgments

We thank and acknowledge Occidental Petroleum Corporation for their support in the acquisition of this important data set. We thank the management of Shell Exploration and Production Company and its affiliates for their permission to publish this paper. We also acknowledge Neubrex Energy Services, LLC, and Neubrex Co., Ltd. for their support in data acquisition, signal processing, and data analysis and interpretation. We thank the Gas Technology Institute for permission to publish data from Hydraulic Fracture Test Site 2.

## References

Binder, G., Titov, A., Tamayo, D. et al. 2019. Time-Lapse Seismic Monitoring of Individual Hydraulic Frac Stages Using a Downhole Distributed Acoustic Sensing Array. Paper presented at the SPE/AAPG/SEG Unconventional Resources Technology Conference, Denver, Colorado, USA, 22–24 July. URTEC-2019-409-MS. https://doi.org/10.15530/urtec-2019-409.

Byerley, G., Monk, D., Aaron, P. et al. 2018. Time-Lapse Seismic Monitoring of Individual Hydraulic Frac Stages Using a Downhole DAS Array. *Lead Edge* **37** (11): 802–810. https://doi.org/10.1190/tle37110802.1.

Cole, S., Karrenbach, M., Kahn, D. et al. 2018. Source Parameter Estimation from DAS Microseismic Data. In *SEG Technical Program Expanded Abstracts 2018*, 4928–4932. Tulsa, Oklahoma, USA: Society of Exploration Geophysicists. https://doi.org/10.1190/segam2018-2995716.1.

Friehauf, K. and Gibson, M. R. 2019. DAS Method of Estimating Fluid Distribution. US Patent No. 10,465,501.

Guzik, A., Yokoyama, M., Matsuda, K. et al. 2013. Monitoring of the Ground Settlement during a Tunnel Excavation Using 4D Optical Fiber Sensing System. In *Fifth European Workshop on Optical Fibre Sensors*, Vol. 8794, 87943H. Bellingham, Washington, USA: International Society for Optics and Photonics. https://doi.org/10.1117/12.2026148.

Haustveit, K., Dahlgren, K., Greenwood, H. et al. 2017. New Age Fracture Mapping Diagnostic Tools: A STACK Case Study. Paper presented at the SPE Hydraulic Fracturing Technology Conference and Exhibition, The Woodlands, Texas, USA, 24–26 January. SPE-184862-MS. https://doi.org/10.2118/184862-MS.

Horiguchi, T., Kurashima, T., and Tateda, M. 1989. Tensile Strain Dependence of Brillouin Frequency Shift in Silica Optical Fibers. *IEEE Photonics Technol Lett* **1** (5): 107–108. https://doi.org/10.1109/68.34756.

Ichikawa, M., Kato, M., Uchida, S. et al. 2020. Low Frequency DAS Data Study with Integrated Data Analysis for Monitoring Hydraulic Fracture. Paper presented at the 82nd EAGE Annual Conference and Exhibition, Virtual, 8–11 December. https://doi.org/10.3997/2214-4609.202011176.

Jin, G., Friehauf, K., Roy, B. et al. 2019. Fiber Optic Sensing-Based Production Logging Methods for Low-Rate Oil Producers. Paper presented at the SPE/AAPG/SEG Unconventional Resources Technology Conference, Denver, Colorado, USA, 22–24 July. URTEC-2019-943-MS. https://doi.org/10.15530/urtec-2019-943.

Jin, G. and Roy, B. 2017. Hydraulic-Fracture Geometry Characterization Using Low-Frequency DAS Signal. *Lead Edge* **36** (12): 975–80. https://doi.org/10.1190/tle36120975.1.

Karrenbach, M., Cole, S., Ridge, A. et al. 2019. Fiber-Optic Distributed Acoustic Sensing of Microseismicity, Strain and Temperature during Hydraulic Fracturing. *Geophysics* **84** (1): D11–D23. https://doi.org/10.1190/geo2017-0396.1.

Karrenbach, M., Kahn, D., Cole, S. et al. 2017. Hydraulic-Fracturing-Induced Strain and Microseismic Using In Situ Distributed Fiber-Optic Sensing. *Lead Edge* **36** (10): 837–844. https://doi.org/10.1190/tle36100837.1.

Kishida, K., Yamauchi, Y., and Guzik, A. 2014. Study of Optical Fibers Strain-Temperature Sensitivities Using Hybrid Brillouin-Rayleigh System. *Photonic Sens* **4** (1): 1–11. https://doi.org/10.1007/s13320-013-0136-1.

Kole, P. R., Cannon, M., Doornhof, D. et al. 2017. First Year of Distributed Strain Sensing in the Groningen Field. Paper presented at the EAGE/DGG Workshop, Potsdam, Germany, 31 March. https://doi.org/10.3997/2214-4609.201700165.

Liu, F., Michael, E., Johansen, K. et al. 2017. Time-Lapse Geochemistry (TLG) Application in Unconventional Reservoir Development. Paper presented at the SPE/AAPG/SEG Unconventional Resources Technology Conference, Austin, Texas, USA, 24–26 July. URTEC-2670186-MS. https://doi.org/10.15530/urtec-2017-2670186.

Liu, F., Wu, J., Jin, M. et al. 2020a. From Reservoir Characterization to Reservoir Monitoring: An Integrated Workflow To Optimize Field Development Using Geochemical Fingerprinting Technology. Paper presented at the SPE/AAPG/SEG Unconventional Resources Technology Conference, Virtual, 20–22 July. URTEC-2020-2902-MS. https://doi.org/10.15530/urtec-2020-2902.

Liu, Y., Wu, K., Jin, G. et al. 2020b. Rock Deformation and Strain-Rate Characterization during Hydraulic Fracturing Treatments: Insights for Interpretation of Low-Frequency Distributed Acoustic-Sensing Signals. *SPE J*. **25** (5): 2251–2264. SPE-202482-PA. https://doi.org/10.2118/202482-PA.

Mali, G. A., Clark, R. R., Kenyon, S. B. et al. 2019. Field Deployment of Fiber Optic Technology To Monitor Overburden Deformation. Paper presented at the SPE Annual Technical Conference and Exhibition, Calgary, Alberta, Canada, 30 September–2 October. SPE-196209-MS. https://doi.org/10.2118/196209-MS.

Maxwell, S. C., Rutledge, J., Jones, R. et al. 2010. Petroleum Reservoir Characterization Using Downhole Microseismic Monitoring. *Geophysics* **75** (5): 75A129–75A137. https://doi.org/10.1190/1.3477966.

Molenaar, M. M., Hill, D., Webster, P. et al. 2012. First Downhole Application of Distributed Acoustic Sensing for Hydraulic-Fracturing Monitoring and Diagnostics. *SPE Drill & Compl* **27** (1): 32–38. SPE-140561-PA. https://doi.org/10.2118/140561-PA.

Pankaj, P. 2018. Characterizing Well Spacing, Well Stacking, and Well Completion Optimization in the Permian Basin: An Improved and Efficient Workflow Using Cloud-Based Computing. Paper presented at the SPE/AAPG/SEG Unconventional Resources Technology Conference, Houston, Texas, USA, 23–25 July. URTEC-2876482-MS. https://doi.org/10.15530/urtec-2018-2876482.

Raterman, K. T., Farrell, H. E., Mora, O. S. et al. 2017. Sampling a Stimulated Rock Volume: An Eagle Ford Example. Paper presented at the SPE/AAPG/SEG Unconventional Resources Technology Conference, Austin, Texas, USA, 24–26 July. URTEC-2670034-MS. https://doi.org/10.15530/urtec-2017-2670034.

Raterman, K. T., Liu, Y., and Warren, L. 2019. Analysis of a Drained Rock Volume: An Eagle Ford Example. Paper presented at the SPE/AAPG/SEG Unconventional Resources Technology Conference, Denver, Colorado, USA, 22–24 July. URTEC-2019-263-MS. https://doi.org/10.15530/urtec-2019-263.

Rezaei, A., Rafiee, M., Siddiqui, F. et al. 2017. The Role of Pore Pressure Depletion in Propagation of New Hydraulic Fractures during Refracturing of Horizontal Wells. Paper presented at the SPE Annual Technical Conference and Exhibition, San Antonio, Texas, USA, 9 October. SPE-187055-MS. https://doi.org/10.2118/187055-MS.

Richter, P., Parker, T., Woerpel, C. et al. 2019. High-Resolution Distributed Acoustic Sensor Using Engineered Fiber for Hydraulic Fracture Monitoring and Optimization in Unconventional Completions. In *SEG Technical Program Expanded Abstracts*, 4874–4878. Tulsa, Oklahoma, USA: Society of Exploration Geophysicists. https://doi.org/10.1190/segam2019-3215860.1.

Stokely, C. L. 2016. Acoustics-Based Flow Monitoring during Hydraulic Fracturing. Paper presented at the SPE Hydraulic Fracturing Technology Conference, The Woodlands, Texas, USA, 9–11 February. SPE-179151-MS. https://doi.org/10.2118/179151-MS.

Titov, A., Binder, G., Liu, Y. et al. 2020. Modeling and Interpretation of Scattered Waves in Inter-Stage DAS VSP Survey. *Geophysics* **86** (2): 1–49. https://doi.org/10.1190/geo2020-0293.1.

Ugueto C. G. A., Wojtaszek, M., Huckabee, P. T. et al. 2018. Accelerated Stimulation Optimization via Permanent and Continuous Production Monitoring Using Fiber Optic. Paper presented at the SPE/AAPG/SEG Unconventional Resources Technology Conference, Houston, Texas, USA, 23–25 July. URTEC-2901897-MS. https://doi.org/10.15530/urtec-2018-2901897.

Ugueto, G., Huckabee, P., Wojtaszek, M. et al. 2019a. New Near-Wellbore Insights from Fiber Optics and Downhole Pressure Gauge Data. Paper presented at the SPE Hydraulic Fracturing Technology Conference and Exhibition, The Woodlands, Texas, USA, 5–7 February. SPE-194371-MS. https://doi.org/10.2118/194371-MS.

Ugueto, G. A., Todea, F., Daredia, T. et al. 2019b. Can You Feel the Strain?: DAS Strain Fronts for Fracture Geometry in the BC Montney, Groundbirch. Paper presented at the SPE Annual Technical Conference and Exhibition, Calgary, Alberta, Canada, 30 September–2 October. SPE-195943-MS. https://doi.org/10.2118/195943-MS.

Vera Rodriguez, I. and Wuestefeld, A. 2020. Strain Microseismics: Radiation Patterns, Synthetics, and Moment Tensor Resolvability with Distributed Acoustic Sensing in Isotropic Media. *Geophysics* **85** (3): KS101–KS114. https://doi.org/10.1190/geo2019-0373.1.

Wang, H. 2016. Poro-Elasto-Plastic Modeling of Complex Hydraulic Fracture Propagation: Simultaneous Multi-Fracturing and Producing Well Interference. *Acta Mechanica* **227** (2): 507–525. https://doi.org/10.1007/s00707-015-1455-7.

Webster, P., Cox, B., and Molenaar, M. 2013. Developments in Diagnostic Tools for Hydraulic Fracture Geometry Analysis. Paper presented at the SPE/AAPG/SEG Unconventional Resources Technology Conference, Denver Colorado, USA, 12–14 August. URTEC-1619968-MS. https://doi.org/10.1190/urtec2013-025.

Xue, Z. and Hashimoto, T. 2017. Geomechanical Monitoring of Caprock and Wellbore Integrity Using Fiber Optic Cable: Strain Measurement from the Fluid Injection and Extraction Field Tests. *Energy Procedia* **114**: 3305–3311. https://doi.org/10.1016/j.egypro.2017.03.1462.

Zhu, J., Forrest, J., Xiong, H. et al. 2017. Cluster Spacing and Well Spacing Optimization Using Multi-Well Simulation for the Lower Spraberry Shale in Midland Basin. Paper presented at the SPE Liquids-Rich Basins Conference–North America, Midland, Texas, USA, 13–14 September. SPE-187485-MS. https://doi.org/10.2118/187485-MS.